

From 3D real structure to 3D modelled structure: Modelling water vapor permeability in polypropylene/cellulose composites



Marouane Kabbej^a, Valérie Guillard^a, Hélène Angellier-Coussy^a, Valentin Thoury-Monbrun^a, Nathalie Gontard^a, Laurent Orgéas^b, Sabine Rolland Du Roscoat^b, Sébastien Gaucel^{a,*}

^a IATE, Univ Montpellier, CIRAD, INRAE, Institut Agro, 34060, Montpellier, France

^b CNRS, Univ. Grenoble Alpes, 3SR Lab, UMR 5521, F-38000, Grenoble, France

ARTICLE INFO

Keywords:
3D numerical modelling
Composites
Interphase

ABSTRACT

A 3D tri-phasic numerical model was developed to predict water vapor permeability in composite materials made of polypropylene (PP) as matrix and cellulose particles as fillers, with existence of an interphase around permeable inclusions. About 70 tri-phasic structures composed of ellipsoidal, heterogenous-size particles were generated to represent composites with four different filler contents ($\varphi_p = 2.96 - 6.06 - 12.67 - 19.91\%v/v$) with interfacial region at the filler/matrix interface (either 1 or 2 μm thick) displaying its own permeability. The relative permeability (i.e., ratio between composite and neat matrix permeability) was calculated from Finite Element Method (FEM) simulations on these structures. A good prediction of experimental relative permeability for the whole filler content range investigated was observed. The presence of a percolating interphase observed in some structures explains the high permeabilization observed for high φ_p . The proposed 3D numerical model was confronted to five state-of-the art analytical models and was the only one able to describe the observed complex structures with identification of reliable characteristics for the interphase (thickness, permeability).

1. Introduction

A composite is a combination of at least two non-miscible components having different properties and with a finite interface between the components. Bi-phasic systems are often considered as a dispersion of particles into a continuous phase, the matrix. Permeability of a gas and vapor, i.e. mass transport phenomenon through a membrane upon difference of gas partial pressure according to Fick theory [1] is essential in many domains of interest of composite materials. Predictive modelling of such property thus receives a lot of interest. One of the original models for bi-phasic systems was proposed in 1873 by Maxwell in his "Treatise on Electricity and Magnetism" [2] to predict electrical conductivity of infinitely diluted clusters of particles embedded in an infinite matrix. It was later extended to mass transfer modelling to relate permeability of the bi-phasic system to the permeability of the matrix and the particles' volume fraction (φ_p). Maxwell's theory, initially developed for very simple bi-phasic system and $\varphi_p \leq 20\%v/v$, was, thereafter, largely updated to consider more complex situations (see for

instance the Chew-Glandt, Lewis-Nielson, Higuchi or Maxwell-Wagner-Sillars models) [3–6] and a little bit later the Bruggeman's theory, applicable to higher filler content than the Maxwell's one, φ_p up to 35%v/v [7].

Following these pioneer works, a lot of work has been carried out - and is still ongoing - to improve these first analytical equations to consider either more complex particle geometry or higher particle volume fraction. Thus, still recently, Papadokostaki et al. [8] proposed an update of the Maxwell equation to make it valid for high φ_p range (up to 100%v/v in theory, e.g., continuous phase) by considering a cubic particle shape instead of spheres. Some authors even proposed analytical tri-phasic models that take into account a third compartment at the particle/matrix interface, i.e., interphase, at the vicinity of filler particles [9–11]. Because the interfacial layer characteristics and, in some cases, additional adjustable fitting constants are necessarily empirically fitted to experimental data, these models including interfacial non-idealities, have been largely shown to match experimental data of permeability in various systems such as mixed matrix membranes

* Corresponding author.

E-mail addresses: marouane.kabbej@umontpellier.fr (M. Kabbej), valerie.guillard@umontpellier.fr (V. Guillard), helene.coussy@umontpellier.fr (H. Angellier-Coussy), valentin.thoury-monbrun@umontpellier.fr (V. Thoury-Monbrun), nathalie.gontard@inrae.fr (N. Gontard), Laurent.Orgreas@3sr-grenoble.fr (L. Orgéas), Sabine.Rolland-Du-Roscoat@univ-grenoble-alpes.fr (S.R. Du Roscoat), sebastien.gaucel@inrae.fr (S. Gaucel).

(MMMs) [9]. However, they do not permit to clearly understand the impact of the interphase. In addition, they do not account for heterogeneity in particle size and in interphase thickness, for potential interphase overlapping and resulting percolation pathways that strongly influence overall mass transfer properties.

To overcome these limitations and with advance in computer capability, many researchers have used numerical simulation method to investigate mass transport into composites. They proposed models that consider the real or rebuilt 2D or 3D structure of the composite system on which coupled partial differential equations (PDEs) describing the transport through the membrane is numerically solved via the Finite Element Method (FEM). Such approach has been largely used for modelling solute diffusion into concrete (see for example the recent work of [12]) or permeability into mixed matrix membranes (MMMs). For instance, Petsi and Burganos [13] proposed a 2D numerical model to study the dependence of MMMs' permeability on the volume fraction of inclusions, of interphase layer, the size of the inclusions, and the permeability values of the three phases. Van Soestbergen et al. [14] developed a 3D tri-phasic model to evaluate the diffusivity of moisture through polymer composites containing impermeable equal-sized spheres that did not participate in the overall diffusion. They concluded that the effective diffusivity does not only depend on the composite tortuosity and the interphase diffusivity, but also on the interphase volume fraction and the formation of interphase aggregates. Monsalve-Bravo et al. [15] developed 3D models considering permeable spherical particles randomly distributed to predict permeability of CO_2 and CH_4 through MMMs. Addition of an interphase (region of modified matrix surrounding the particles) of constant thickness, less permeable than the bulk matrix, allowed to decrease the numerical permeability of the MMM and thus to match the experimental data. More recently, Kabbej et al. [16] proposed a 3D tri-phasic numerical model to predict water vapor permeability in a composite made of a continuous polymeric matrix containing permeable spheroidal inclusions. The 3D structures were generated using experimental particles' size distribution from 2D image analysis that has permitted to capture as much variability of the experimental material as possible. The presence of an interphase with adjustable diffusivity but sorption property like that of the matrix value, has permitted to well predict the experimental relative permeabilities. However, in all the studies mentioned above, the models did not gather at the same time all the criteria required to model transfer in tri-phasic systems containing highly permeable, heterogeneous size distributed particles with aggregation, interphase overlapping and percolating structures, which limits their usefulness for real composite systems.

To go beyond state of the art, the objective of this work was to develop a 3D tri-phasic model to predict water vapor permeability in composites. The model was validated on a composite made of a continuous polymeric phase (polypropylene) containing dispersed permeable particles (cellulose) with four different particle volume fractions, $\varphi_p = 2.9, 6.06, 12.67$ and $19.91\%v/v$. 3D structures were generated from 3D tomographic images that provided three-dimensional information on the particles' shape, size and dispersion, which was never done before in state-of-the-art approaches. Such approach should permit to generate simplified but meso- and microscopic well-founded structures. The numerical relative permeabilities (i.e., ratio between composite and neat matrix permeability P_c / P_m) were confronted with experimental ones. The new developed 3D model was then used to numerically explore the impact of the composite structure on the overall permeability, in particular the interphase layer and percolation phenomenon. Finally, the relevance of our 3D model was discussed in relation to existing tri-phasic analytical models.

2. Materials and methods

2.1. Materials

A composite structure consisting of polypropylene (PP) matrix and cellulose particles was considered in this work. Polypropylene (PP) used as matrix was the PH9020 grade supplied from Total Petrochemical. As reported by the manufacturer, it was a homopolymer with a melting temperature of $165\text{ }^\circ\text{C}$ and a density of 0.905 g cm^{-3} . The cellulose used was pure cellulose (cellulose content of 99.5 wt%) and was provided by J. Rettenmaier & Söhne (JRS) (Germany) under the named Arbocel® BE600-10 Tg. According to the manufacturer, cellulose particles had an average particle length of $18\text{ }\mu\text{m}$, an average particle diameter of $15\text{ }\mu\text{m}$ and an apparent density of $0.23\text{--}0.3\text{ g cm}^{-3}$. The true density of cellulose, measured by pycnometry, was $1.56 \pm 0.08\text{ g cm}^{-3}$.

2.2. Preparation of the composite films

Composite films with about 5, 10, 20 and 30 wt % of cellulose were produced in a twin-screw extruder with a centerline distance of 15.6 mm, a screw length of 624 mm and a screw length to diameter ratio L/D of 40 (Prism Eurolab 16XL from Thermo Scientific, Germany). The extruder was assembled with a calendar die to produce plane sheets. Two film thicknesses were tested: $100 \pm 18\text{ }\mu\text{m}$ and $350 \pm 45\text{ }\mu\text{m}$. The global flow rate was 1 kg h^{-1} and the screw speed was 200 rpm. The barrel temperature conditions from the polymer feeding to the die ranged from $120\text{ }^\circ\text{C}$ to $190\text{ }^\circ\text{C}$. A passive event was placed just before the die to degas water vapor that could remain in cellulose particles. A dedicated gravimetric feeder was used to control cellulose feeding rate (Brabender loss-in-weight, twin screw feeder DDW-MD1-MT2) while a volumetric feeder was used to feed PP pellets (Brabender single screw volumetric feeder DSR28). Before extrusion, cellulose samples were dried at $60\text{ }^\circ\text{C}$ for 72 h.

The exact weight cellulose content in biocomposites was determined by thermogravimetric analysis, which was carried out using a Mettler TGA2 apparatus. The initial sample weight was around 10 mg. Samples were heated from $25\text{ }^\circ\text{C}$ to $800\text{ }^\circ\text{C}$ at a constant rate of $10\text{ }^\circ\text{C}\text{ min}^{-1}$ under air flow (50 mL min^{-1}). Cellulose content on each composite was calculated from the mass loss between $250\text{ }^\circ\text{C}$ and $400\text{ }^\circ\text{C}$, which was related to thermal degradation of cellulose. From $420\text{ }^\circ\text{C}$ to $550\text{ }^\circ\text{C}$, thermal degradation was related to polypropylene. Experiments were performed in triplicate. The volume fraction of cellulose in biocomposites was deduced from this measurement knowing the true density of cellulose and that of PP.

2.3. Water vapor permeability (WVP)

Water vapor permeability (WVP) of films was gravimetrically determined at $23\text{ }^\circ\text{C}$ with a relative humidity gradient from 0 to 100% using a modified ASTM procedure (ASTM E96 – Standard test methods for water vapor transmission of materials). Samples were hermetically sealed with Teflon seals in glass permeation cells containing distilled water. The free film surface was 9.08 cm^2 . Cells were placed in a desiccator containing silica gel to have around 0% of relative humidity (RH). Thus, a RH gradient equal to 100% was considered by assuming that the RH of silica gel was exactly 0%. Water vapor transfer, w , (g day^{-1}) through the exposed film area, A (m^2), was measured from the cell weight loss as a function of time (five replicants). WVP was calculated from the following equation:

$$WVP = \frac{|w| \cdot e}{A \cdot \Delta p \cdot 3600 \cdot M_{H_2O}} \quad \text{Eq. 1}$$

where e is the thickness (m), Δp (Pa) is the differential pressure between both sides of the film and M_{H_2O} is the molecular weight of water ($M_{H_2O} = 18.016\text{ g mol}^{-1}$).

2.4. Experimental parameters for water vapor transfer modelling

Water vapor diffusivity and sorption characteristics in the polymer and cellulose particles were previously obtained and recalled hereafter.

- The effective moisture diffusivities D [$\text{m}^2 \cdot \text{s}^{-1}$] in PP matrix and in cellulose particles are $(1.32 \pm 0.33) \times 10^{-12}$ [17] and $(5.84 \pm 1.37) \times 10^{-12} \text{ m}^2 \cdot \text{s}^{-1}$ respectively [18].
- The boundary conditions for the composite (supposed to be neat matrix solely) are dry air on one side and saturated humid air on the other side, corresponding to the measurement of permeability between 0 and 100% of relative humidity. It corresponds to a concentration of water on the polymer surface of 0 and $161.08 \text{ mol} \cdot \text{m}^{-3}$ respectively, calculated using the experimental water vapor sorption isotherm curve of PP measured previously at 20°C [17]. The maximal water vapor sorption derived from the curve at 100% RH is $3.21 \pm 1.11 \times 10^{-3} \text{ g}$ of water g^{-1} dry basis. This data was converted in mol m^{-3} using the water molar mass of 18 g mol^{-1} and the PP density of 0.905 g cm^{-3} .
- The water vapor partition coefficient K , calculated as the slope of the linear relation between the water concentration in PP matrix and cellulose particles, obtained from experimental water vapor sorption isotherm at 20°C [17] for PP matrix and cellulose particles, is $K = 137.77$ [-].

2.5. 3D X-ray computed tomography

Microtomographic images of $1844 \times 1403 \times 298 \mu\text{m}^3$ (length x depth x thickness) of the PP/cellulose composite with $\varphi_p = 2.96 \%v/v$ were obtained by using X-ray microtomography on the ID19 beamline at the ESRF in Grenoble with a resolution of $0.65 \mu\text{m}^3/\text{voxel}$.

2.6. From 3D X-ray computed tomographic image analysis to 3D structure generation

The 3D composite structures were generated using the cascading (3D) reconstruction procedure of a composite material from microCT data described in Methods X. Structural descriptors of cellulose particles were extracted from 3D tomographic image. Cellulose particles were assimilated to either spheres and ellipsoids whose shape descriptors were measured using MorphoLibJ plugin in ImageJ software [19]. Ellipsoids were characterized by the three axes, a_1 , largest axis, a_2 , medium axis and, a_3 , smallest axis and three orientation angles, named Tait-Bryan angles with x-y-z extrinsic rotation convention: ψ , roll angle, θ , elevation angle and, φ , azimuth angle. Spheres were characterized by the diameter d . The experimental distribution of these descriptors was fitted by Kernel distribution laws.

Generation of bi-phasic and tri-phasic structures. The MATLAB code developed for generating 3D structures was based on Tschopp MATLAB code [20]. The code generated 3D microstructures composed of a population of non-overlapping ellipsoidal particles heterogeneously distributed in size and orientation, within a periodic RVE. Same code could be used for spheres.

Bi-phasic structures. The composite structure was generated in a cuboid shaped representative volume element (RVE) defined by $(x, y, z) \in [0, L_x] \times [0, L_y] \times [0, L_z]$, where z is the overall diffusion direction. The RVE was supposed periodic along its vertical faces, to represent an infinite repetitive structure along x and y axis. The cuboid shape was selected in order to keep as the $[0, L_z]$ dimension, the whole thickness of the composite membrane studied. Structure generation required the RVE size and the target particles volume fraction $\varphi_{p,\text{target}}$ as inputs.

Particle geometric parameters were randomly generated using the selected distribution law (Kernel) until the total particle volume fraction reached the target, using the stop criterion $|\varphi_{p,\text{target}} - \varphi_p| \leq 0.01 \%v/v$.

Then, these particles were sequentially positioned and oriented in

the periodic RVE by randomly generating both the position of particle's centre (i.e., centre coordinates x_c, y_c, z_c) and the orientation angles (ψ, θ, φ). The addition of a new particles to the structure was made by ensuring that there was non-overlapping of the particle with the horizontal faces of the RVE ($z = 0$ and $z = L_z$) and with the existing particles (see Methods X for detailed procedure). It should be noted that if a particle intercepted one of the vertical faces of the RVE then, the particle section outside from the RVE was shifted to the opposite face, to ensure the periodicity of the RVE (Fig. 1a).

Tri-phasic structures. The tri-phasic composite structure was built by considering an interphase of fixed thickness around each particle of the already generated bi-phasic structures. The interphase volume was thus different for each particle, keeping constant the initial particle volume. For the interphase compartment, the periodicity at vertical faces of the RVE still applies. For particles close to the upper (resp. lower) face of the RVE, the interphase may intercept the boundary. In that case, the intercept with the exterior of the RVE was removed (Fig. 1b).

It is important to note that once the 3D structures were generated on Matlab with Tait-Bryan angles (ψ, θ, φ), the latter were converted to the classical Euler angles (γ, β, α) to be integrated in Comsol for upcoming simulation.

2.7. Mathematical modelling and geometry of the 3D model

a. Governing Equations

Mass transfer in the composite is described by Fick's second law of diffusion in both the matrix Ω_m and the particle Ω_p domains for the bi-phasic system (Fig. 1a) and in the interphase domain Ω_i for the tri-phasic system (Fig. 1b). In stationary regime and in the absence of mass source, this law is expressed by the following partial differential:

$$\operatorname{div}\left(\vec{J}_k\right)=0 \quad \text{Eq. 2}$$

with

$$\vec{J}_k(x, y, z) = -D_k \vec{\nabla} c_k(x, y, z) \quad \text{Eq. 3}$$

where index k stands for the domain considered, matrix (m), particle (p) or interphase (i), $D_k [\text{m}^2 \cdot \text{s}^{-1}]$ is the diffusivity in domain k , considered constant (not concentration/temperature/time dependent), \vec{J}_k the molar surface flux vector [$\text{mol} \cdot \text{m}^{-2} \cdot \text{s}^{-1}$] depending on the concentration c_k [$\text{mol} \cdot \text{m}^{-3}$] of water vapor in the domain k .

b. Boundary Conditions

Periodic boundary conditions were imposed on the vertical side boundaries of the RVE, which consisted of imposing equality of concentration and flux on the so-called 'source' and 'destination' boundaries (Fig. 1a). The periodic boundary conditions allowed simulating an infinite repetitive structure.

Bi-phasic system. Constant concentrations were imposed on the upper face $\partial\Omega^{m,\text{upper}}$ and the lower face $\partial\Omega^{m,\text{lower}}$ of the matrix (Eq. (4) & Fig. 1a). Particles' domain was assumed to not overlap the upper and lower horizontal faces of the RVE.

$$c_m > 0 \text{ at } \partial\Omega^{m,\text{upper}} \text{ and } c_m = 0 \text{ at } \partial\Omega^{m,\text{lower}} \quad \text{Eq. 4}$$

The concentration is discontinuous ($c_m \neq c_p$) at the matrix-particle boundary $\partial\Omega^{m,p}$ where the dimensionless partition coefficient $K = c_p / c_m$ is considered. To get continuous flux at the matrix-particle boundary $\partial\Omega^{m,p}$, a special type of boundary condition using the stiff-spring method [21] was applied:

$$\left(-\vec{J} \cdot \vec{n}\right)_m = M(c_p - K \cdot c_m) \text{ at } \partial\Omega^{m/p} \quad \text{Eq. 5}$$

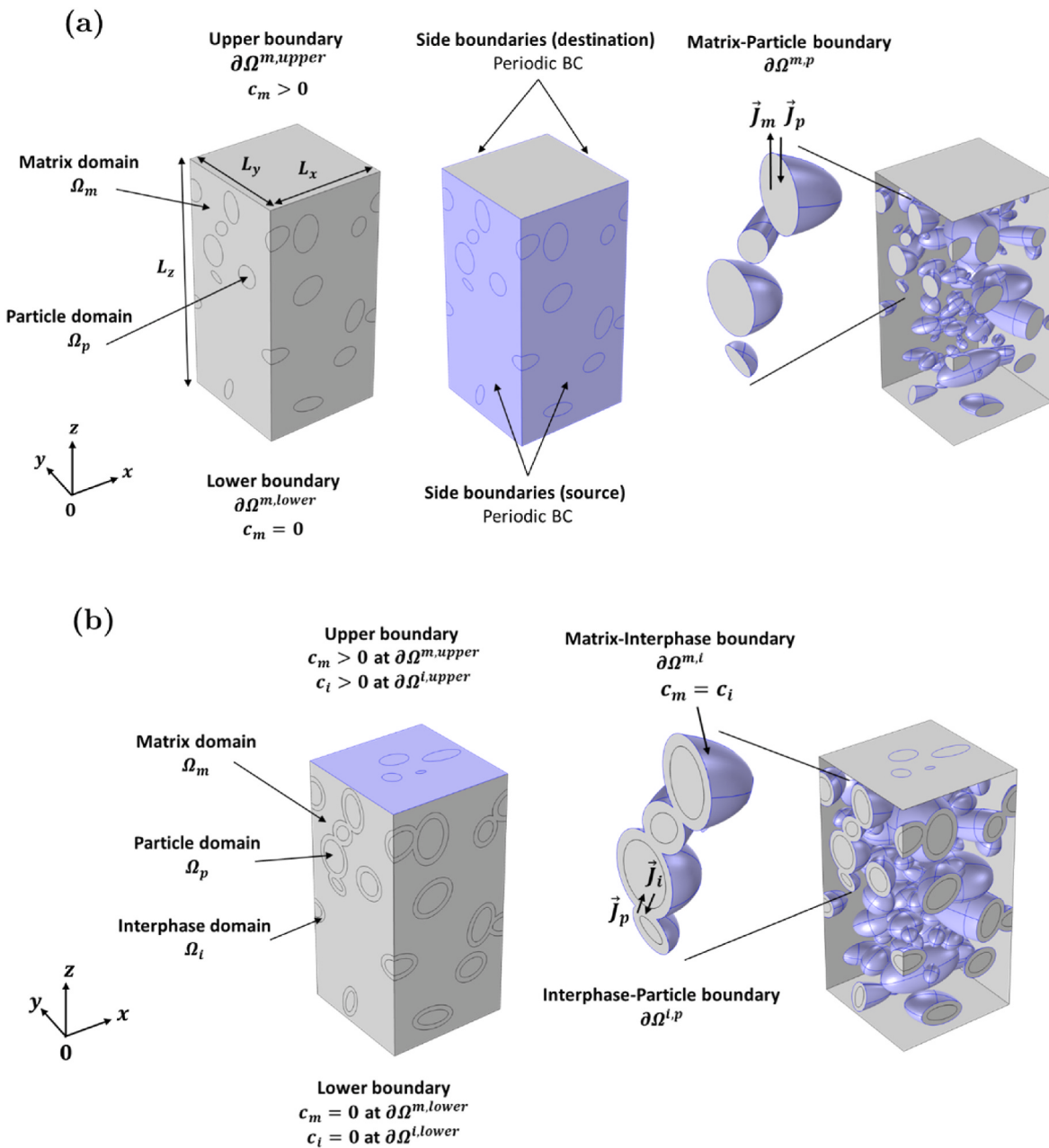


Fig. 1. Representation of the RVE showing: (a) the boundaries conditions at the six composite faces and at the matrix-particle boundary for a bi-phasic structure; (b) the boundaries conditions at the upper and lower composite faces, the matrix-interphase and interphase-particle boundaries for a tri-phasic structure.

$$\left(-\vec{J} \cdot \vec{n} \right)_p = M(K \cdot c_m - c_p) \text{ at } \partial\Omega^{p/m} \quad \text{Eq. 6}$$

where M is a (non-physical) velocity [$m \cdot s^{-1}$] large enough to let the concentration differences in the brackets approach zero, thereby satisfying $K = c_p/c_m$. This boundary condition gives a continuous flux across the boundaries, if M is sufficiently large. In all simulations, M was taken equal to 1000 m.s^{-1} .

Tri-phasic system. Interphase domain was considered as matrix with degraded diffusivity values. Therefore, interphase was supposed to have the same sorption properties as the matrix. In addition, contrary to particles, interphase could overlap the upper and lower horizontal faces of the RVE. Constant concentrations were imposed on the upper face ($\partial\Omega^{m,upper}, \partial\Omega^{i,upper}$) and the lower face ($\partial\Omega^{m,lower}, \partial\Omega^{i,lower}$) of the matrix and interphase (Eqs. (7) and (8) & Fig. 1b):

$$c_m = c_i > 0 \text{ at } \partial\Omega^{m,upper} \text{ and } \partial\Omega^{i,upper} \quad \text{Eq. 7}$$

$$c_m = c_i = 0 \text{ at } \partial\Omega^{m,lower} \text{ and } \partial\Omega^{i,lower} \quad \text{Eq. 8}$$

Continuity of concentration was applied at the matrix-interphase boundary $\partial\Omega^{m,i}$:

$$c_m = c_i \text{ at } \partial\Omega^{m,i} \quad \text{Eq. 9}$$

At the interphase-particle boundary $\partial\Omega^{i,p}$, the same condition previously applied for the bi-phasic system was adopted with partition coefficient $K = c_p/c_i$. The boundary conditions using the stiff-spring method in the three-phase system are thus:

$$\left(-\vec{J} \cdot \vec{n} \right)_i = M(c_p - K \cdot c_i) \text{ at } \partial\Omega^{i/p} \quad \text{Eq. 10}$$

$$\left(-\vec{J} \cdot \vec{n} \right)_p = M(K \cdot c_i - c_p) \text{ at } \partial \Omega^{p/i} \quad \text{Eq. 11}$$

where M is the same as above.

c. Effective Permeability Evaluation

The numerical solving of the boundary value problem gave the molar concentration field $c_i(x, y, z)$ [$\text{mol} \cdot \text{m}^{-3} \cdot \text{s}^{-1}$] and the molar surface flux vector field $\vec{J}(x, y, z)$ [$\text{mol} \cdot \text{m}^{-2} \cdot \text{s}^{-1}$] of the permeating specie at the discretization points of each domain Ω_k ($k = m, p, i$). The molar flux φ_z [$\text{mol} \cdot \text{s}^{-1}$] (along z-axis) across the upper ($z = L_z$), middle ($z = L_z/2$) and lower ($z = 0$) cross-sections was calculated by:

$$\varphi_z(z) = \int_0^{L_x} \int_0^{L_y} J_z(x, y, z) dx dy \quad \text{Eq. 12}$$

where J_z is the molar surface flux (along z-axis) at the discretization points. Then, the effective permeability [$\text{mol} \cdot \text{m}^{-2} \cdot \text{s}^{-1} \cdot \text{Pa}^{-1}$] of the micro-composite was finally given by:

$$P = \frac{\varphi_z}{L_x \times L_y} \left(\frac{L_z - 0}{P_{upper} - P_{lower}} \right) \quad \text{Eq. 13}$$

where $L_x \times L_y$ is the surface of the faces [m^2], L_z is the RVE thickness [m], P_{upper} and P_{lower} are the water vapor pressure [Pa] imposed on the upper ($z = L_z$) and the lower ($z = 0$) faces of the RVE respectively and φ_z is the molar flux [$\text{mol} \cdot \text{s}^{-1}$].

2.8. COMSOL model and numerical simulations

The 3D problem of diffusion was solved by using the numerical Finite Element Method (FEM) using COMSOL Multiphysics 5.5 software. For mass diffusion simulation, the “Transport of Diluted Species” physics interface of the “Chemical Reaction Engineering” module was used, which already integrates the 2nd Fick’s law equation. To support the complex geometry of tri-phasic structures and avoid mesh errors, the COMSOL CAD Import module was used. The simulations were performed using a DELL computer with Intel Xeon E-2176 M Processor (2.7 GHz) and 32 Gb of Ram. The entire computational procedure (from structure generation to simulation) was driven within the MATLAB environment and was partially automated via the COMSOL LiveLink for MATLAB module (from the step of importing geometry data into COMSOL to simulation).

As previously demonstrated [16] and checked in the current work (see Section S1 in Supp. Material), ten structures per case study were considered acceptable in the following to achieve reliable calculation of numerical relative permeability.

For the discretization of the composite geometry, a mesh consisting of tetrahedral elements of [0.15–3.5] μm (predefined in COMSOL) was used. Preliminary simulations performed on 40 bi-phasic and tri-phasic structures of RVE size of $50 \times 50 \times 100 \mu\text{m}^3$ with heterogeneous ellipsoidal particles, revealed that globally the best convergence of solutions was obtained with this tetrahedral mesh element size (see Section S2 in Supp. material).

Preliminary simulations performed on about 100 structures with heterogeneous ellipsoidal particles and particles volume fraction of $\varphi_p = 2.96 \%v/v$ including bi-phasic ($e_i = 0 \mu\text{m}$) and tri-phasic structures ($e_i = 2.5 \mu\text{m}$) for different RVE sizes ($50 \times 50 \times 100$), ($100 \times 100 \times 100$), ($200 \times 200 \times 100$) μm^3 have revealed that the RVE size did not significantly impact the solution of permeability (see Section S3 in Supp. material). Therefore, a minimal RVE of $50 \times 50 \times 100 \mu\text{m}^3$ was chosen for all further simulations, permitting in addition to achieve reasonable computational time.

3. Results and discussion

3.1. Numerical prediction of water vapor permeability in tri-phasic structures

3.1.1. A- 3D structure reconstruction

The microCT-data were acquired for the PP/cellulose composite loaded with the lowest cellulose volume content, i.e. $\varphi_p = 2.96 \%v/v$. A total of 12 812 particles was analysed. The average experimental axis lengths were $a_1 = 11.57 \pm 9.87$, $a_2 = 6.83 \pm 4.77$ and $a_3 = 4.35 \pm 2.43 \mu\text{m}$ which is a bit lower than the median major and minor axis previously measured on isolate cellulose particles, $19 \pm (2.1)$ and $11 \pm (1.5) \mu\text{m}$ respectively [22]. A truncated Kernel law was used to randomly generate particle descriptors (i.e. sizes and orientation angles). 15 000 particles were generated to check the reliability of this procedure by comparing experimental distribution to the simulated one (see details in Methods X). Using previous distribution laws, about ten bi-phasic and ten tri-phasic structures were generated for each filler content ($\varphi_p = 2.96 - 6.06 - 12.67 - 19.91 \%v/v$) and interphase thickness ($e_i = 0, 1, 2 \mu\text{m}$), leading to more than 120 structures in total. Examples of 3D tri-phasic structures of different filler content are shown in Fig. 2. These structures were a basis to compute water vapor flux and water vapor permeability.

3.1.2. b. permeability predictions: effect of increasing particles volume fraction on the permeability by the presence of interphase

As shown in Fig. 3, the bi-phasic approach was not able to reproduce the experimental relative permeabilities on the entire range of filler volume fraction. Between $\varphi_p = 2.96 \%v/v$ and $\varphi_p = 6.06 \%v/v$ experimental relative permeability sharply increased then tend to stagnate up to $\varphi_p = 12.67 \%v/v$ before sharply inflect up to $\varphi_p = 19.91 \%v/v$. This sigmoid shape is somewhere unexpected and the inflection between $\varphi_p = 2.96$ and $\varphi_p = 6.06 \%v/v$ is probably due to uncontrolled defects in the composite membrane. However, the exponential increase of the relative permeability with particle volume fraction is obvious. Below $\varphi_p = 12.67 \%v/v$ predicted relative permeabilities follow a linear and slowly increasing trend which more or less follows the evolution of experimental relative permeability. But for higher φ_p , the model was not able to catch the inflection experimentally observed between $\varphi_p = 12.67 \%v/v$ and $\varphi_p = 19.91 \%v/v$. This strong permeabilization at high φ_p would be mostly due to interfacial non-idealities, which are poorly described using ideal models [9,15,16]. This confirms the importance to directly integrate interphase in 3D numerical approaches.

The interphase is characterized by its thickness e_i and diffusivity D_i . Two different interphase thicknesses were considered, $e_i = 1 \mu\text{m}$ and $e_i = 2 \mu\text{m}$ in agreement with interphase thickness range of the literature. Indeed, among the different references found in the literature about interphase thickness, either calculated or measured by nanoindentation for instance – both given similar results – different ranges of thickness were found, all in the same order of magnitude: 1–4 μm in glass fibre/epoxy composite [23,24], from few nanometers up to 10 μm [25] or 0.8–1.5 μm [26] in glass fibre/silane measured by nanoscratch test, from 0.6 to 2.2 μm depending on the fibre volume fraction [27], or from 5 to 6 μm in natural fibres reinforced poly (lactic acid) biocomposites [28]. First simulations were performed with an interphase diffusivity $D_i = 3.58 \times 10^{-12} \text{ m}^2 \cdot \text{s}^{-1}$, an intermediate value between D_m and D_p . That means that the interphase is more diffusive than the matrix ($D_i > D_m$), which seems logical and in line with the “permeabilization” effect observed at high filler volume fractions. This is usually commonly observed in the literature especially when particle agglomeration leads to the presence of non-selective interfacial voids in the composite membrane as observed by Vu et al. [29] in nanodiamonds/Pebax matrix where interfacial permeability was calculated twice that of the neat Pebax membrane. With an interphase of several micrometres, Woo and Piggott [30] have shown that the interphase diffusion coefficient should

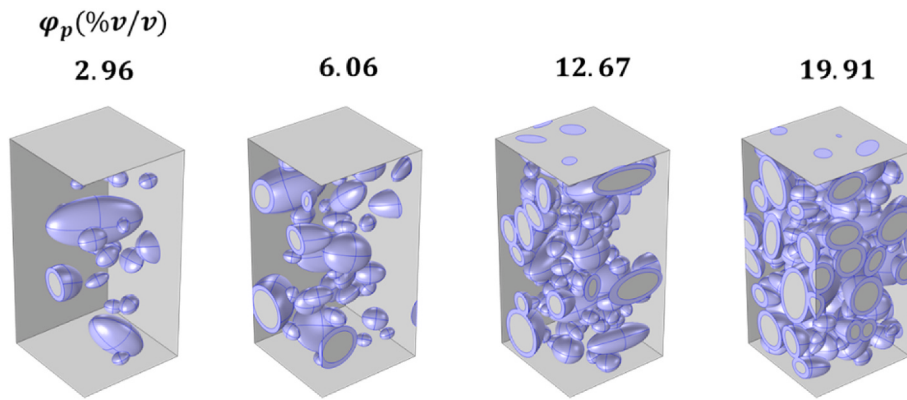


Fig. 2. Examples of 3D composite tri-phasic structures ($50 \times 50 \times 100 \mu\text{m}^3$) generated by considering heterogenous ellipsoidal particles and volume fractions corresponding to true composite materials ($\varphi_p = 2.96 - 6.06 - 12.67 - 19.91 \%v/v$). The interphase ($e_i = 2 \mu\text{m}$) is highlighted in purple color. (For interpretation of the references to colour in this figure legend, the reader is referred to the Web version of this article.)

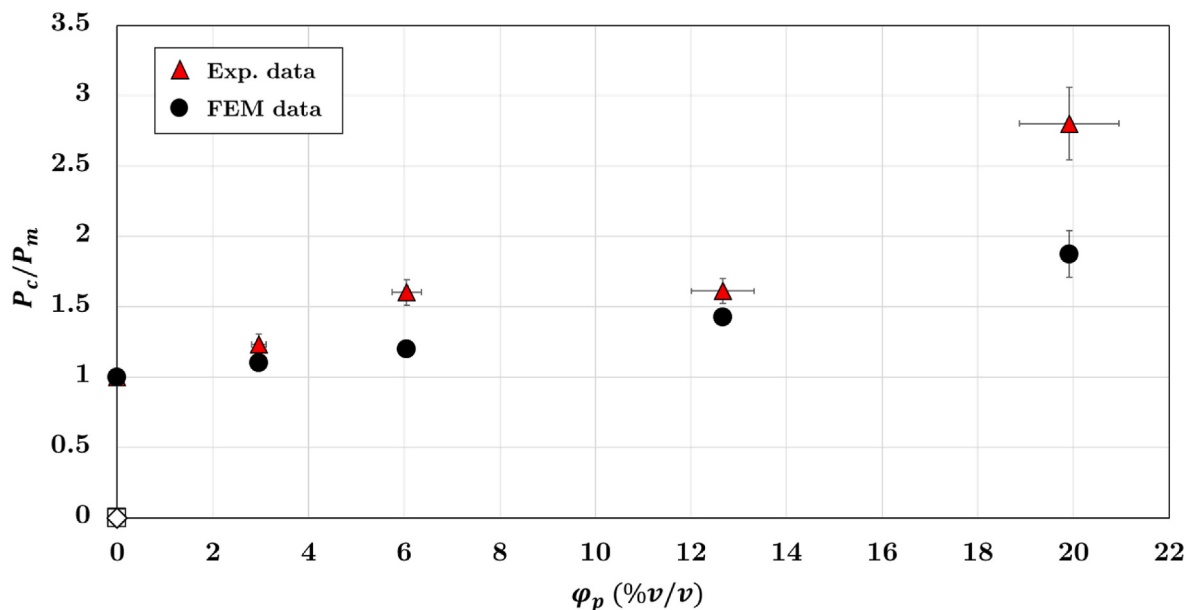


Fig. 3. Comparison between experimental and numerical relative permeability P_c/P_m . The numerical data correspond to the mean of the relative permeability of at least 10 (3D) bi-phasic structures.

be 10 times that of D of the bulk matrix and Joliff et al. [23] observed a $D_i = 7 \times D_m$ in their work on epoxy resin/glass fibres composite. In the present case, $D_i \approx 3 \times D_m$ which is slightly lower than the D_i to D_m ratios found in the literature.

For an interphase layer of 1 μm or 2 μm and $D_i \approx 3 \times D_m$, a good representation of the evolution of the experimental relative permeability as a function of the particles' volume fraction was obtained (Fig. 4, round black symbols). Interphase of 2 μm is more prone to well predict relative permeability at high volume fraction while the interphase of 1 μm is more suitable for lower filler fraction, where permeabilization effect seems less important. The appropriate couple (interphase thickness and interphase diffusivity) probably lies in between. There is no reason either why there should be a single couple of values suitable for the whole filler volume fraction range. In addition, it must be acknowledged that if both interphase thickness and diffusivity were chosen to keep constant the overall transport resistance, $R_i = \frac{e_i}{D_i}$, same simulation of relative permeability for the composite should theoretically be obtained as observed by Vu et al. [29]. However, this effect which is well observed on diluted systems with non-contacting particles [29], deserves to be explored on concentrated systems when percolating

interphases exist.

3.2. Comparison between 3D numerical simulations and analytical tri-phasic models

The 3D tri-phasic model was then compared to analytical tri-phasic models from the literature. Five tri-phasic analytical models whose expressions are detailed in Table 1 were selected. The tri-phasic models are by nature more complex than the analytical bi-phasic models because they consider in addition to P_m , P_p and φ_p , two other parameters P_i (interphase permeability) and φ_i (interphase volume fraction) that characterise the interphase:

$$\frac{P_c}{P_m} = f(P_m, P_p, \varphi_p, P_i, \varphi_i, \dots) \quad \text{Eq. 14}$$

To apply these models to our data, several input parameters were required, notably permeability values for the matrix and the particle. The water vapor permeability for the PP matrix and cellulose particles, P_m and P_p , were calculated as the product of experimental diffusivity by experimental solubility ($P = D \times S$), both obtained from the dynamic

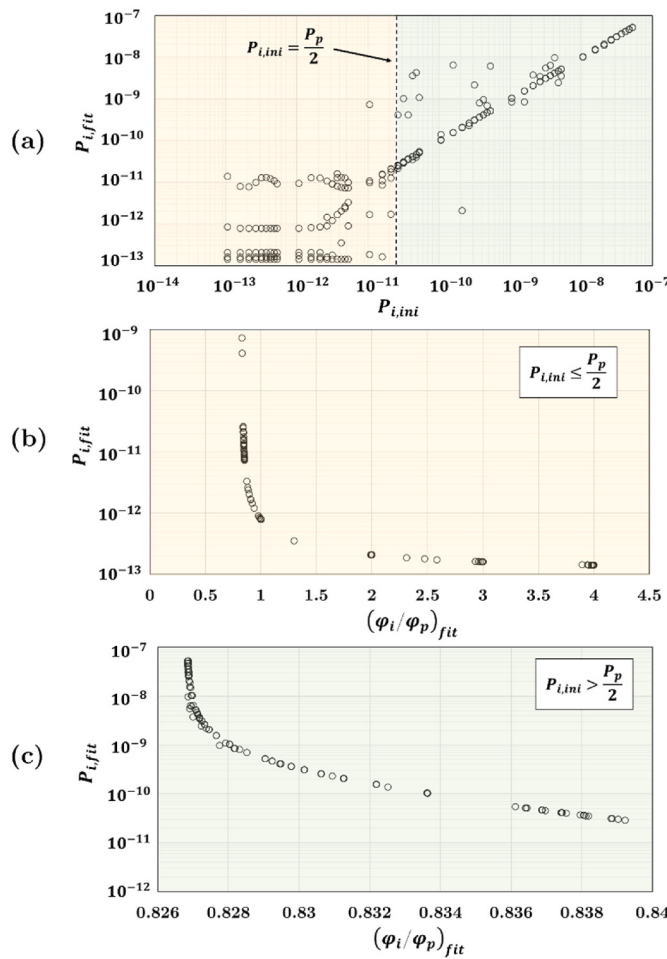


Fig. 4. Parameter estimation of the pseudo-bi-phasic Maxwell model on experimental water vapor permeability of PP/cellulose. (a) Behavior of the estimated interphase permeability $P_{i,fit}$ depending on its initial value $P_{i,ini}$. Two zones are separated by the dashed line corresponding to $P_{i,ini} = P_p/2$. (b) & (c) Behavior of the fitted $P_{i,fit}$ according to the fitted $(\varphi_i/\varphi_p)_{fit}$ when $P_{i,ini} \leq P_p/2$ and $P_{i,ini} > P_p/2$ respectively.

sorption experiments at 20 °C previously performed in our laboratory [17]. Values of D_m and D_p were those used for the matrix and particles in our 3D numerical model. The obtained values of permeability were $P_m = 0.91 \times 10^{-13}$ and $P_p = 522.5 \times 10^{-13} \text{ mol}\cdot\text{m}\cdot\text{m}^{-2}\cdot\text{s}^{-1}\cdot\text{Pa}^{-1}$.

P_i could be either higher than P_m when there are interfacial voids between the matrix and particles or lower when polymer rigidification occurs near the particle surface [31]. P_i is usually identified by fitting the model to experimental data. This is the strategy selected in a first test in our next work.

The analytical models considered in this work are the pseudo-bi-phasic Maxwell model (Eq. 1.1–1.3), the pseudo-bi-phasic Maxwell-Wagner-Sillars model (Eq. 1.4–1.6), the pseudo-bi-phasic Lewis-Nielsen model (Eq. 1.7–1.9), Felske model (Eq. 1.10) and the modified Felske model (Eq. 1.11) (Table 1). All these models used as descriptors the interphase permeability P_i , volume fraction φ_i or thickness e_i , and in some cases, one additional parameter such as for instance the maximum volume packing fraction of particles, $\varphi_{p,\max}$ such as in the pseudo-bi-phasic Lewis-Nielsen or the modified Felske models. The Felske and modified Felske models contain the ratio δ of the radius of the spherical pseudo-particle to the radius of the spherical particle: $\delta = (r_p + e_i)/r_p$, where r_p is the sphere radius. Only the Maxwell-Wagner-Sillars model considers spheroids, and the other theoretical models consider spherical particles. That's why the pseudo-bi-phasic Maxwell-Wagner-Sillars

model contains the geometrical factor n as additional parameter. None of these models consider aggregation or particle size distributions.

In the following, $\varphi_{p,\max}$, which corresponds to random close packing of particles [36], was fixed to $\varphi_{p,\max} = 70\% \text{ v/v}$ in the pseudo-bi-phasic Lewis-Nielsen and modified Felske models and was supposed to be the same for the particles and the pseudo-particles. In the Maxwell-Wagner-Sillars model n was supposed to be the same for the particles (Eq. 1.4) and the pseudo-particles (Eq. 1.5)."

First test. The five analytical tri-phasic models were confronted to experimental data. Parameter estimation was performed on the two parameters defining the interphase, $(P_i, \varphi_i/\varphi_p)$, plus one additional parameter (n or δ) when considered in the analytical model. Estimation procedure, based on root mean squared error (RMSE) minimization, required initial guess for the unknown parameters, and as recommended to avoid local minima, several sets of initial guesses were considered. The analytical models seemed efficient since the obtained RMSE values were in the range [0.163; 0.173] (see Section S4 in Supp. material) however the estimated parameters have no possible physical interpretation for the following reasons. First, apart for the pseudo-bi-phasic Lewis-Nielsen model, there was no unicity of the estimated parameters. For each model, we obtained a lot of sets of optimal parameters presenting the same RMSE (no less than 270 number of combinations for the Maxwell model or 1326 for the pseudo-bi-phasic Maxwell Wagner Sillars, up to 5400 for the Felske's one) (see Section S4 in Supp. material). It is well illustrated for the pseudo-bi-phasic Maxwell model in Fig. 4 showing how identified interphase permeability, P_i , could vary depending on the value given for its initialization in the optimisation algorithm or on the ratio of interphase volume fraction to particle volume fraction (φ_i/φ_p) that is fitted simultaneously to P_i . It was thus not possible to define the characteristic of the interphase without additional information using such basic fitting of analytical equations with multiple, simultaneous, parameters adjustment.

Second, the range of parameters obtained, especially for P_i and in a lesser extent for φ_i , were very large and gave no information. For instance, the interphase permeability can be indifferently taken to value from 10^{-13} to $10^{-8} \text{ mol}\cdot\text{m}\cdot\text{m}^{-2}\cdot\text{s}^{-1}\cdot\text{Pa}^{-1}$, and, with the *ad hoc* value for φ_i , as shown in Fig. 4b–c for the pseudo-bi-phasic Maxwell model (see also Table S4.1 in Supp. Material), one can obtain a satisfactory fit with experimental data. Again, it gave no physically exploitable information on P_i .

Also, we observed that the effective permeability P_c was preferentially sensitive to a particular parameter and not to the others leading to bias into the fitting procedure. The same problem was observed by Moore et al. [37] when they estimated the chain immobilization factor β , related to P_i ($P_i = P_m/\beta$), and the interphase thickness e_i by fitting the permeability of the pseudo-bi-phasic Maxwell model to experimental O_2 and CO_2 permeabilities in a system where polymer rigidification occurs near the filler particle surface. Fig. 4-a shows the estimated interphase permeability $P_{i,fit}$ versus its initial value $P_{i,ini}$ for the pseudo-bi-phasic Maxwell model. It is worth remembering that for each initial value $P_{i,ini}$, we ran several parameter estimations with several values for $\varphi_{i,ini}$ and so several $(P_{i,ini}, \varphi_{i,ini})$ initial guess. For low values of $P_{i,ini}$, it led to several candidates for $P_{i,fit}$ (Fig. 4-a), as previously mentioned. For high values of $P_{i,ini}$, most of the estimated values followed the relationship $P_{i,fit} = P_{i,ini}$ (Fig. 4-a), capturing the fact that P_i has no effect on P_c calculation. This latter drawback can be explained by a simple mathematical analysis. Indeed, when $P_i \gg P_p, P_m$, the pseudo-bi-phasic Maxwell model degenerates into a single equation (Eq. (15)) which depends only on φ_{pi} , so on φ_p and φ_i .

$$\frac{P_c}{P_m} = \frac{1 + 2\varphi_{pi}}{1 - \varphi_{pi}} \quad \text{Eq. 15}$$

Finally, even if the considered analytical triphasic models were able to reproduce the experimental data, with filler fraction up to 20 v/v%, they were unable to provide physical insight on the interphase since a

Table 1

Description of the five analytical models used in the present work to model permeability in tri-phasic composites.

Model	Expression	Additional expression	Parameters
Pseudo-bi-phasic Maxwell [32,33]	Phase (pi) = Particles (p) + Interphase (i) $\frac{P_{pi}}{P_i} = \frac{2(1 - \varphi_p') + (1 + 2\varphi_p') \frac{P_p}{P_i}}{(2 + \varphi_p') + (1 - \varphi_p') \frac{P_p}{P_i}}$ (Eq. 1.1) Global system = Phase (pi) + Matrix (m) $\frac{P_c}{P_m} = \frac{2(1 - \varphi_{pi}) + (1 + 2\varphi_{pi}) \frac{P_{pi}}{P_m}}{(2 + \varphi_{pi}) + (1 - \varphi_{pi}) \frac{P_{pi}}{P_m}}$ (Eq. 1.2) $\frac{P_c}{P_m} \approx \frac{1 + 2\varphi_{pi}}{1 - \varphi_{pi}} \text{ for } P_i \gg P_p \gg P_m$ (Eq. 1.3)	Phase (pi) = Particles (p) + Interphase (i) $\varphi_p' = \frac{V_p}{V_p + V_i} = \frac{\varphi_p}{\varphi_p + \varphi_i}$ Global system = Phase (pi) + Matrix (m) $\varphi_{pi} = \frac{V_p + V_i}{V_p + V_i + V_m} = \varphi_p + \varphi_i$	φ_p' : Particles volume fraction in the phase (pi) φ_{pi} : Particles plus Interphase volume fraction in the whole system φ_p : Particles volume fraction in the whole system φ_i : Interphase volume fraction in the whole system
Pseudo-bi-phasic Maxwell-Wagner-Sillars [9,34]	Phase (pi) = Particles (p) + Interphase (i) $\frac{P_{pi}}{P_i} = \frac{n P_p + (1 - n) P_i - (1 - n)(P_i - P_p)\varphi_p'}{n P_p + (1 - n) P_i + n(P_i - P_p)\varphi_p'}$ (Eq. 1.4) Global system = Phase (pi) + Matrix (m) $\frac{P_c}{P_m} = \frac{n P_{pi} + (1 - n) P_m - (1 - n)(P_m - P_{pi})\varphi_{pi}}{n P_{pi} + (1 - n) P_m + n(P_m - P_{pi})\varphi_{pi}}$ (Eq. 1.5) $\frac{P_c}{P_m} \approx \frac{1 + n(1 - \varphi_{pi})}{n(1 - \varphi_{pi})} \text{ for } P_i \gg P_p \gg P_m$ (Eq. 1.6)	Phase (pi) = Particles (p) + Interphase (i) $\varphi_p' = \frac{V_p}{V_p + V_i} = \frac{\varphi_p}{\varphi_p + \varphi_i}$ Global system = Phase (pi) + Matrix (m) $\varphi_{pi} = \frac{V_p + V_i}{V_p + V_i + V_m} = \varphi_p + \varphi_i$	$\varphi_p, \varphi_{pi}, \varphi_p', \varphi_i$ are the same than Pseudo-bi-phasic Maxwell model. n : Geometrical factor of the particle
Pseudo-bi-phasic Lewis-Nielsen [5]	Phase (pi) = Particles (p) + Interphase (i) $\frac{P_{pi}}{P_i} = \frac{1 + 2\beta\varphi_p'}{1 - \psi\beta\varphi_p'}$ (Eq. 1.7) Global system = Phase (pi) + Matrix (m) $\frac{P_c}{P_m} = \frac{1 + 2\beta\varphi_{pi}}{1 - \psi\beta\varphi_{pi}}$ (Eq. 1.8) $\frac{P_c}{P_m} = \frac{1 + 2\varphi_{pi}}{1 - \psi\varphi_{pi}} \text{ for } P_i \gg P_p \gg P_m$ (Eq. 1.9)	Phase (pi) = Particles (p) + Interphase (i) $\varphi_p' = \frac{V_p}{V_p + V_i} = \frac{\varphi_p}{\varphi_p + \varphi_i}$ $\psi = 1 + \left(\frac{1 - \varphi_{p,max}}{\varphi_{p,max}^2}\right)\varphi_p'$ Global system = Phase (pi) + Matrix (m) $\varphi_{pi} = \frac{V_p + V_i}{V_p + V_i + V_m} = \varphi_p + \varphi_i$ $\psi = 1 + \left(\frac{1 - \varphi_{p,max}}{\varphi_{p,max}^2}\right)\varphi_{pi}$ $\beta = \frac{P_i - 1}{P_p + 2}$ with $-\frac{1}{2} \leq \beta \leq 1$	$\varphi_p', \varphi_{pi}, \varphi_p, \varphi_i$ are the same than Pseudo-bi-phasic Maxwell model. $\varphi_{p,max}$: Maximum packing volume fraction of particles
Felske [10,35]	$\frac{P_c}{P_m} = \frac{2(1 - \varphi_{pi}) + (1 + 2\varphi_{pi})(\eta/\gamma)}{(2 + \varphi_{pi}) + (1 - \varphi_{pi})(\eta/\gamma)}$ (Eq. 1.10)	$\eta = (2 + \delta^3)\left(\frac{P_p}{P_m}\right) - 2(1 - \delta^3)\left(\frac{P_i}{P_m}\right)$ $\gamma = 1 + 2\delta^3 - (1 - \delta^3)\left(\frac{P_p}{P_i}\right)$ for $P_i \gg P_p \gg P_m$ $\eta \approx -2(1 - \delta^3)\left(\frac{P_i}{P_m}\right)$ $\gamma \approx 1 + 2\delta^3$ $\varphi_{pi} = \frac{\varphi_p}{\varphi_p + [(1 - \varphi_p)/\delta^3]}$ $\delta = \frac{r_{pi}}{r_p} = \frac{r_p + e_i}{r_p}$ $\varphi_{pi} = \varphi_p + \varphi_i$	φ_{pi} : Particles plus interphase volume fraction in the whole system φ_p : Particles volume fraction in the whole system φ_i : Interphase volume fraction in the whole system δ : Ratio of outer radius of interface to the core particle one
Modified Felske [11]	$\frac{P_c}{P_m} = \frac{1 + 2((\eta - \gamma)/(\eta + 2\gamma))\varphi_p}{1 - ((\eta - \gamma)/(\eta + 2\gamma))\varphi_p\psi}$ (Eq. 1.11)	Same parameters than Felske model $\psi = 1 + \left(\frac{1 - \varphi_{p,max}}{\varphi_{p,max}^2}\right)\varphi_p$	$\varphi_{pi}, \varphi_p, \varphi_i, \delta$ are the same than Felske model. $\varphi_{p,max}$: Maximum packing volume fraction of particles

unique solution for (P_i, φ_i) could not be achieved.

Second test. To decrease the degree of freedom and the number of parameters to be fitted, P_i and φ_i were fixed based on our previous 3D numerical modelling. The water vapor permeability for the interphase P_i was calculated as the product of the interphase diffusivity identified in the 3D model by the experimental matrix solubility ($P_i = D_i \times S_m$), considering that the interfacial phenomena affected only the polymer diffusivity in the vicinity of the particles $D_i \neq D_m$ and not the sorption coefficient $S_i = S_m$. The obtained value of interphase permeability is $P_i = 2.47 \times 10^{-13} \text{ mol} \cdot \text{m}^{-2} \cdot \text{s}^{-1} \cdot \text{Pa}^{-1}$ with $P_m < P_i < P_p$.

The interphase volume fraction, φ_i , was fixed to the value calculated from the 3D structures generated for each φ_p studied. As at least 10

structures were generated per φ_p , at least 10 values of φ_i were then considered per φ_p and the tri-phasic analytical models were then run for each φ_i .

Once φ_i and P_i were fixed, the geometrical factor n was fitted to experimental data (pseudo-bi-phasic Maxwell-Wagner-Sillars model). The δ parameter (Felske and modified Felske models) was fixed based on the outer radius of the interface and core particle radius extracted from the 3D generated structures with size-heterogeneous spherical particles. For this purpose, a set of 40 structures (about 10 structures for each φ_p) were built with spheres whose diameters were randomly drawn following a truncated Kernel distribution fitted to the real distribution of the diameters of the equivalent spheres, in volume, of the real particles

(see Methods X). The fixed value of δ (reported in Table 2), related to the diameter, is the mean of all δ calculated for each spherical particle of the 3D generated structures of size-heterogeneous spheres for each φ_p .

Once additional parameters were fixed, relative permeabilities were calculated, one per φ_i and then averaged to obtain a single relative permeability value per φ_p . Since φ_i varies as a function of e_i , the permeabilities obtained for $e_i = 1 \mu\text{m}$ are different from those obtained for $e_i = 2 \mu\text{m}$. Based on values obtained for $e_i = 2 \mu\text{m}$, best RMSE values were achieved for FEM model > Pseudo-bi-phasic Maxwell-Wagner-Sillars model > Pseudo-bi-phasic Maxwell model > Pseudo-bi-phasic Lewis-Nielsen model > Modified Felske model > Felske model.

As shown in Fig. 5b and Table 2, the present 3D tri-phasic numerical model with $e_i = 2 \mu\text{m}$ is the closest to experimental data. By reducing their degree of freedom and limiting the number of fitting parameters, the tri-phasic analytical deviated a bit more from the experimental results than in the first case where all adjustable parameters were fitted altogether. However, considering an interphase thickness of $2 \mu\text{m}$, at least two of the algebraic models have quite similar prediction to the FEM simulation results. However, one must keep in mind that these good results were obtained because the FEM simulation results gave valuable insights on composite morphology and properties (Π was fixed and φ_i was deduced from FEM results). In the present case study, the algebraic equations could not be used alone without previously deep understanding of the composite morphology using a FEM approach. The algebraic models proved that they are not able to be explanatory and that their parameters are not reliable enough to describe complex structures. The same observation was made by Monsalve-Bravo et al. [15] when comparing some existing tri-phasic models (Pseudo-bi-phasic Maxwell, Bruggeman and Chiew-Glandt models and Felske model) to their own 3D tri-phasic numerical model. As a conclusion, the analytical tri-phasic models can be predictive but not explanatory, while our 3D numerical model can be both.

3.3. Impact of percolation on the relative permeability

The higher permeability value obtained for the highest experimental filler volume fraction investigated, $\varphi_p = 19.91 \%v/v$, could be explained by the presence of percolating network formed by the overlapped in-

Table 2

Resulting fitting parameters and deviation error of the tri-phasic numerical and analytical models (second test) for water vapor permeability in PP/cellulose composite. The 1st and the 2nd lines correspond to $e_i = 1 \mu\text{m}$ and $e_i = 2 \mu\text{m}$ respectively.

Model	e_i	Parameters (* estimated values)	RMSE
3D FEM tri-phasic model	$e_i = 1 \mu\text{m}$	-	0.276
	$e_i = 2 \mu\text{m}$	0.151	
Pseudo-bi-phasic Maxwell-Wagner-Sillars	$e_i = 1 \mu\text{m}$	$n = 0.21^*$	0.179
	$e_i = 2 \mu\text{m}$	$n = 0.28^*$	0.174
Pseudo-bi-phasic Maxwell	$e_i = 1 \mu\text{m}$	-	0.369
	$e_i = 2 \mu\text{m}$	0.212	
Pseudo-bi-phasic Lewis-Nielsen	$e_i = 1 \mu\text{m}$	-	0.221
	$e_i = 2 \mu\text{m}$	0.219	
Modified Felske	$e_i = 1 \mu\text{m}$	$\delta = 1.39 (\varphi_{p,\max} = 0.70)$	0.444
	$e_i = 2 \mu\text{m}$	$\delta = 1.79 (\varphi_{p,\max} = 0.70)$	0.343
Felske	$e_i = 1 \mu\text{m}$	$\delta = 1.39$	0.487
	$e_i = 2 \mu\text{m}$	$\delta = 1.79$	0.421

terphases where the migrant could diffuse totally from one side to the other side of the composite as illustrated in Fig. 6.

To support the presence of a percolating interphase, an example of a 2D cross-sectional grayscale image of the 3D tomographic image of PP/cellulose composite of $\varphi_p = 27.89 \%v/v$ (40%wt in mass fraction) is presented in Fig. 7. Even if the discontinuous phase (white), representing the cellulose particles, did not appear very clear, we could observe the proximity between the particles and the important presence of aggregates that could be described as contact and/or overlapping between particles and/or interphase.

4. Conclusion

In this paper, a 3D tri-phasic modelling approach was proposed to improve the understanding of the relationships between structure and mass transfer properties in composite with highly permeable particles and interphase. Ellipsoidal particles of heterogeneous sizes for different composites of $\varphi_p = 2.96 - 6.06 - 12.67 - 19.91 \%v/v$ were considered for numerical simulations. Results revealed that considering an interphase of $2 \mu\text{m}$ in the 3D structures was essential to correctly predict the macroscopic relative permeability for the studied composite of high φ_p . Our work also highlighted that the analytical models of the literature globally failed to correctly characterise this interphase. By fitting so many parameters all together (i.e., interphase permeability P_i , interphase volume fraction φ_i etc.), they completely lose their meaning and representativeness. By reducing their degree of freedom by fixing some values such as interphase permeability and volume fraction, they completely deviated from the experimental values. The presence of high diffusive percolating interphase, observed in some 3D tri-phasic structures, explains the high experimental permeabilization for high φ_p .

Funding

This project has received funding from the European Union's Horizon 2020 research and innovation program under grant agreement No 773375.

3SR is part of the labex Tec 21 (ANR-11-LBX-0030) and of Institute Carnot Polynat (ANR-16-CARN-0025-01).

CRediT authorship contribution statement

Marouane Kabbej: Investigation, Methodology, Software, Writing – original draft. **Valérie Guillard:** Supervision, Writing – review & editing, Project administration, Funding acquisition. **Hélène Angellier-Coussy:** Supervision, Resources, Formal analysis. **Valentin Thoury-Monbrun:** Investigation, Methodology. **Nathalie Gontard:** Resources, Conceptualization, Funding acquisition. **Laurent Orgéas:** Formal analysis, Writing – review & editing. **Sabine Rolland Du Roscoat:** Formal analysis, Writing – review & editing. **Sébastien Gaucel:** Methodology, Writing – review & editing, Data curation.

Declaration of competing interest

The authors declare that they have no known competing financial interests or personal relationships that could have appeared to influence the work reported in this paper.

Data availability

Data available on a dedicated dataverse.

Size distribution of cellulose particles into PP/cellulose particles <https://doi.org/10.57745/PDQNR6>.

Descriptors of the cellulose particles detected in the 3D microtomography images of composites PP/cellulose <https://doi.org/10.57745/KXPWXK>.

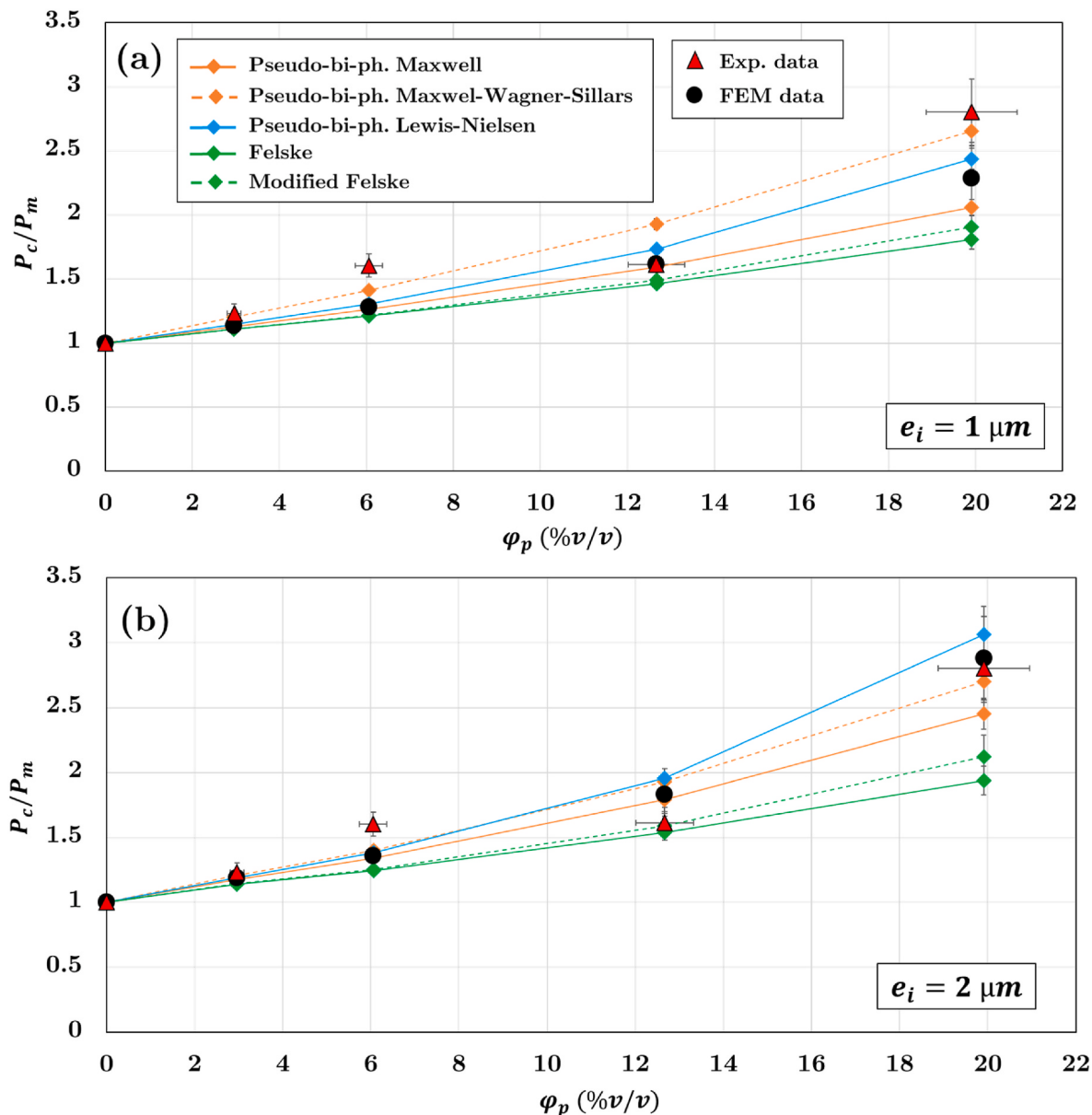


Fig. 5. Comparison between experimental, numerical and analytical relative permeability P_c/P_m . The numerical data are obtained using the tri-phasic model, with an interphase thickness of (a) $e_i = 1 \mu\text{m}$, (b) $e_i = 2 \mu\text{m}$. Water vapor diffusivity in the interphase was arbitrary set to $D_i = 3.58 \times 10^{-12} \text{ m}^2 \cdot \text{s}^{-1}$. The numerical data in this figure correspond to the mean of the relative permeability of at least 10 structures. Five tri-phasic analytical models quoted in Table 1 are evaluated and are added on this figure.

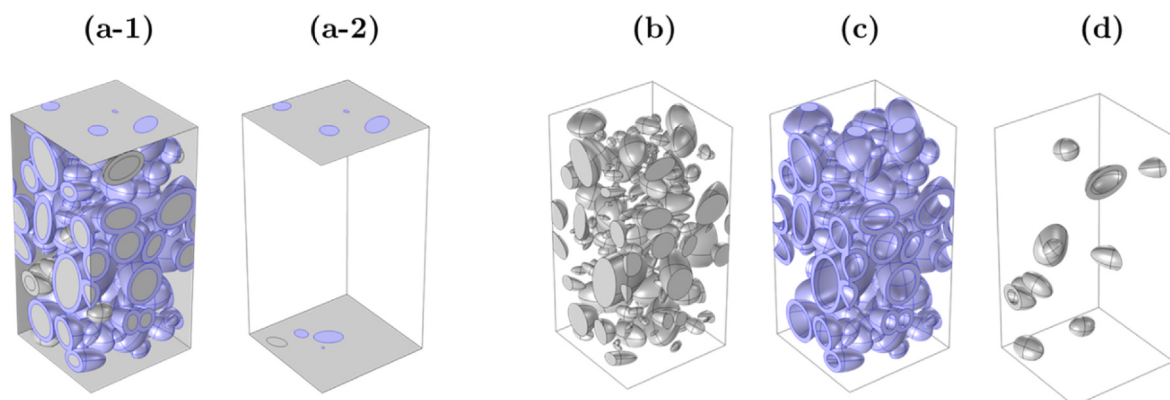


Fig. 6. An example of 3D percolating structure for $\phi_p = 19.91 \%v/v$ (a) with size-heterogeneous ellipsoidal particles (b) and interphase of thickness $e_i = 2 \mu\text{m}$ (c & d). The percolating interphase showed by purple color (a-1) represents a volumetric path of interphases (c) overlapping the RVE upper and lower faces (a-2). The remaining non-percolating interphase is represented in (d). (For interpretation of the references to colour in this figure legend, the reader is referred to the Web version of this article.)

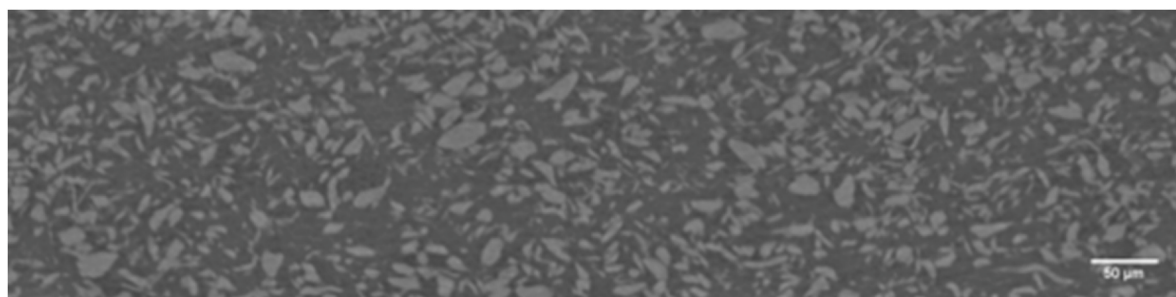


Fig. 7. Example of a 2D cut of the 3D tomographic image of PP/cellulose composite of 40%wt in mass fraction ($\varphi_p = 27.89 \%v/v$) presenting the entire real film thickness of 195 μm (vertical length in the image).

Nomenclature

Abbreviations

RVE	Representative Volume Element
FEM	Finite Element Method
PP	PolyPropylene
2D, 3D	Two and Three Dimension

Latin symbols

L_x, L_y, L_z	RVE length along x -axis, y -axis and z -axis (m)
a_1, a_2, a_3	Major, minor and third axis of the particle (m)
x_c, y_c, z_c	Centre coordinates of the particle (m)
D_k	Diffusivity of water vapor in the phase k ($\text{m}^2 \cdot \text{s}^{-1}$)
P_k	Permeability of water vapor in the phase k ($\text{mol} \cdot \text{m} \cdot \text{m}^{-2} \cdot \text{s}^{-1} \cdot \text{Pa}^{-1}$)
P_c	Permeability of water vapor in the composite ($\text{mol} \cdot \text{m} \cdot \text{m}^{-2} \cdot \text{s}^{-1} \cdot \text{Pa}^{-1}$)
c_k	Concentration of water vapor in the phase k ($\text{mol} \cdot \text{m}^{-3}$)
\vec{J}_k	Molar surface flux vector of water vapor in the phase k ($\text{mol} \cdot \text{m}^{-2} \cdot \text{s}^{-1}$)
$P_{upper} - P_{lower}$	Water vapor pressure differential across the film (Pa)
K	Partition coefficient: concentration ratio between particles and matrix at equilibrium (c_p / c_m) (–)
M	Velocity (non-physical property) ($\text{m} \cdot \text{s}^{-1}$)
e_i	Interphase thickness (m)
n_p	Number of particles (–)

Greek symbols

φ_k	Volume fraction of the phase k: ratio between the volume of the phase k and the composite volume ($\%v/v$)
φ_z	Molar flux (along z -axis) of water vapor across a composite face ($\text{mol} \cdot \text{s}^{-1}$)
ψ	Roll angle corresponding to the first rotation of ellipsoid about the spaced-fixed x -axis and belonging to the Tait-Bryan angles (degree°)
θ	Elevation angle corresponding to the second rotation of ellipsoid about the spaced-fixed y -axis and belonging to the Tait-Bryan angles (degree°)
φ	Azimuth angle corresponding to the third rotation of the ellipsoid about the spaced-fixed z -axis and belonging to the Tait-Bryan angles (degree°)
γ	Intrinsic angle corresponding to the first rotation of ellipsoid about the spaced-fixed z -axis and belonging to the classical Euler angles (degree°)
β	Nutation angle corresponding to the second rotation of ellipsoid about the spaced-fixed x -axis and belonging to the classical Euler angles (degree°)
α	Precession angle corresponding to the third rotation of ellipsoid about the spaced-fixed z -axis and belonging to the classical Euler angles (degree°)

Subscripts

m	Matrix
p	Particle
i	Interphase

Appendix A. Supplementary data

Supplementary data to this article can be found online at <https://doi.org/10.1016/j.polymer.2023.125672>.

References

- [1] A. Fick, On liquid diffusion, *J. Membr. Sci.* 100 (1855) 33–38.
- [2] J.C. Maxwell, *A Treatise on Electricity and Magnetism*, 1873.
- [3] Y.C. Chiew, E.D. Glandt, The effect of structure on the conductivity of a dispersion, *J. Colloid Interface Sci.* 94 (1983) 90–104.
- [4] W.I. Higuchi, T. Higuchi, Theoretical analysis of diffusional movement through heterogeneous barriers, *J. Am. Pharmaceut. Assoc.* 49 (1960) 598–606, <https://doi.org/10.1002/jps.3030490910>.
- [5] T. Lewis, L. Nielsen, Dynamic mechanical properties of particulate-filled composites, *J. Appl. Polym. Sci.* 14 (1970) 1449–1471.
- [6] H. Fricke, The maxwell-wagner dispersion in a suspension of ellipsoids 57 (1951) 934–937.
- [7] D.A.G. Bruggeman, Berechnung verschiedener physikalischer Konstanten von heterogenen Substanzen. I. Dielektrizitätskonstanten und Leitfähigkeiten der Mischkörper aus isotropen Substanzen, *Ann. Phys.* 416 (1935) 636–664, <https://doi.org/10.1002/andp.19354160705>.
- [8] K.G. Papadokostaki, M. Minelli, F. Doghieri, J.H. Petropoulos, A fundamental study of the extent of meaningful application of Maxwell's and Wiener's equations to the permeability of binary composite materials. Part II: a useful explicit analytical approach, *Chem. Eng. Sci.* 131 (2015) 353–359, <https://doi.org/10.1016/j.ces.2015.03.031>.
- [9] G.M. Monsalve-Bravo, Modeling permeation through mixed-matrix membranes: a review, *Processes* 6 (2018), <https://doi.org/10.3390/pr6090172>.
- [10] J.D. Felske, Effective thermal conductivity of composite spheres in a continuous medium with contact resistance, *Int. J. Heat Mass Tran.* 47 (2004) 3453–3461.
- [11] R. Pal, Permeation models for mixed matrix membranes, *J. Colloid Interface Sci.* 317 (2008) 191–198, <https://doi.org/10.1016/j.jcis.2007.09.032>.
- [12] J. Sun, J. Xie, Y. Zhou, Y. Zhou, A 3D three-phase meso - scale model for simulation of chloride diffusion in concrete based on ANSYS, *Int. J. Mech. Sci.* 219 (2022), 107127, <https://doi.org/10.1016/j.ijmecsci.2022.107127>.
- [13] A.J. Petsi, V.N. Burganos, Interphase layer effects on transport in mixed matrix membranes, *J. Membr. Sci.* 421–422 (2012) 247–257, <https://doi.org/10.1016/j.memsci.2012.07.021>.
- [14] M. Van Soestbergen, A. Herrmann, S.J.F. Erich, O.C.G. Adan, Effect of interfacial transport on the diffusivity of highly filled polymers, *Colloid Interface Sci. Commun.* 42 (2021), 100405, <https://doi.org/10.1016/j.colcom.2021.100405>.
- [15] G.M. Monsalve-bravo, R.C. Dutta, S.K. Bhatia, Microporous and Mesoporous Materials Multiscale simulation of gas transport in mixed-matrix membranes with interfacial polymer rigidification, *Microporous Mesoporous Mater.* 296 (2020), 109982, <https://doi.org/10.1016/j.micromeso.2019.109982>.
- [16] M. Kabbej, V. Guillard, H. Angellier-Coussy, C. Wolf, N. Gontard, S. Gaucel, 3D modelling of mass transfer into bio-composite, *Polymers* 13 (2021), <https://doi.org/10.3390/polym13142257>.
- [17] V. Thoury, Formalisation des relations structure/propriétés de transfert de matière dans un biocomposite modèle, *Thèse, Univ. Montpellier*, 2018.
- [18] V. Thoury-Monbrun, S. Gaucel, N. Gontard, V. Guillard, H. Angellier-Coussy, Adapting gravimetric sorption analyzer to estimate water vapor diffusivity in micrometric size cellulose particles, *Cellulose* 26 (2019) 8575–8587, <https://doi.org/10.1007/s10570-019-02661-0>.
- [19] D. Legland, I. Arganda-carreras, P. Andrej, MorphoLibJ : integrated library and plugins for mathematical morphology with ImageJ, *Bioinformatics* 32 (2016) 3532–3534, <https://doi.org/10.1093/bioinformatics/btw413>.
- [20] M.A. Tschopp, 3-D synthetic microstructure generation with ellipsoid particles 3-D synthetic microstructure generation with ellipsoid particles by mark A Tschopp, Report, <https://doi.org/10.13140/RG.2.2.19120.66560>, 2017.
- [21] COMSOL Multiphysics, Separation through dialysis. https://www.comsol.com/forum/thread/attachment/18083/dialysis_sbs-230.pdf, 2008.
- [22] V. Thoury, S. Gaucel, V. Rouessac, V. Guillard, H. Angellier-Coussy, Assessing the potential of quartz crystal microbalance to estimate water vapor transfer in micrometric size cellulose particles, *Carbohydr. Polym.* 190 (2018) 307–314, <https://doi.org/10.1016/j.carbpol.2018.02.068>.
- [23] Y. Joliff, L. Belec, J.F. Chailan, Modified water diffusion kinetics in an unidirectional glass/fibre composite due to the interphase area : experimental , analytical and numerical approach, *Compos. Struct.* 97 (2013) 296–303, <https://doi.org/10.1016/j.compstruct.2012.09.044>.
- [24] M.-B. Heman, Contribution à l'étude des interphases et de leur comportement au vieillissement hydrothermique dans les systèmes à matrice thermodorçissable renforcés de fibres de verre, *Université du Sud Toulon*, 2008.
- [25] J.-K. Kim, A. Hodzic, Nanoscale characterisation of thickness and properties of interphase in polymer matrix composites, *J. Adhes.* 79 (2010) 383–414, <https://doi.org/10.1080/00218460309585>.
- [26] J. Kim, M. Sham, J. Wu, Nanoscale characterisation of interphase in silane treated glass ® bre composites, *Composer Part A*. 32 (2001) 6076–6618.
- [27] M. Lagache, A. Agbossou, J. Pastor, D. Muller, Role of interphase on the elastic behavior of composite materials: theoretical and experimental analysis, *J. Compos. Mater.* 28 (1994) 1140–1157, <https://doi.org/10.1177/002199839402801205>.
- [28] N. Le Moigne, M. Longerey, J. Taulemesse, J. Bénézet, A. Bergeret, Study of the interface in natural fibres reinforced poly (lactic acid) biocomposites modified by optimized organosilane treatments, *Ind. Crop. Prod.* 52 (2014) 481–494, <https://doi.org/10.1016/j.indcrop.2013.11.022>.
- [29] M. Vu, G.M. Monsalve-bravo, R. Lin, M. Li, S.K. Bhatia, S. Smart, Mitigating the agglomeration of nanofiller in a mixed matrix membrane by incorporating an interface agent, *Membranes* 11 (2021) 328.
- [30] M. Woo, M. Piggott, Water absorption of resins and composites: IV. Water transport in fiber reinforced plastics, *J. Compos. Technol. Res.* 10 (1988).
- [31] T.T. Moore, W.J. Koros, Non-ideal effects in organic-inorganic materials for gas separation membranes, *J. Mol. Struct.* 739 (2005) 87–98, <https://doi.org/10.1016/j.molstruc.2004.05.043>.
- [32] R. Mahajan, W.J. Koros, Mixed matrix membrane materials with glassy polymers. Part 1, *Polym. Eng. Sci.* 42 (2002) 1420–1431, <https://doi.org/10.1002/pen.11041>.
- [33] R. Mahajan, W.J. Koros, Mixed matrix membrane materials with glassy polymers . Part 2, *Polym. Eng. Sci.* 42 (2002) 1432–1441, <https://doi.org/10.1002/pen.11042>.
- [34] S. Rafiq, A. Maulud, Z. Man, M. Ibrahim, A. Mutualib, F. Ahmad, A.U. Khan, A. L. Khan, M. Ghauri, N. Muhammad, Modelling in mixed matrix membranes for gas separation, *Can. J. Chem. Eng.* 93 (2015) 88–95, <https://doi.org/10.1002/cjce.22111>.
- [35] S.A. Hashemifarid, A.F. Ismail, T. Matsuura, Prediction of gas permeability in mixed matrix membranes using theoretical models, *J. Membr. Sci.* 347 (2010) 53–61, <https://doi.org/10.1016/j.memsci.2009.10.005>.
- [36] C. Guo, L. Zhou, J. Lv, Effects of expandable graphite and modified ammonium polyphosphate on the flame-retardant and mechanical properties of wood flour-polypropylene composites, *Polym. Polym. Compos.* 21 (2013) 449–456, <https://doi.org/10.1002/app>.
- [37] T.T. Moore, S. Damle, P.J. Williams, W.J. Koros, Characterization of low permeability gas separation membranes and barrier materials; design and operation considerations, *J. Membr. Sci.* 245 (2004) 227–231, <https://doi.org/10.1016/j.memsci.2004.07.017>.